Wind Energy

WIND ENERGY
Wind Energ. (2015)
Published online in Wiley Online Library (wileyonlinelibrary.com). DOI: 10.1002/we.1832

RESEARCH ARTICLE

Another engineering wake model variant for horizontal axis wind turbines

Michael J. Werle†

Ogin Inc., Waltham, Massachusetts 02453, USA

ABSTRACT

An engineering model is presented for predicting the performance of a single turbine located in an incoming turbulent, sheared, wind velocity field. The approach used is a variant of the well-known and documented Ainslie eddy viscosity approach as also employed in the Direct Wake Meandering model. It incorporates a new and simple means of representing the rotor's loading profile, initializing the calculations, simplifying the wakes' shear layer mixing model and accounting for wind shear effects. Additionally, two figures of merit are employed for assessing the reliability of all data used and predictions provided. The first, a wake momentum-flux/thrust parameter, is used for quantitatively assessing the accuracy and utility of both measured and/or computational wake data. The second, a rotor swept area wake-averaged velocity, is employed as a single quantitative measure of a turbine's impact on its downstream neighbor. Through detailed comparisons with three independent state-of-the-art Computational Fluid Dynamic generated datasets and a field-measured dataset, the current model is shown to be accurate for turbine rated power levels from 100 kW to 2.3 MW, wind speeds of 6 to 22 m s^{-1} (corresponding to turbine thrust coefficient levels of 0.14 to 0.8) and free-stream turbulence levels from 0% to 16%. Copyright © 2015 John Wiley & Sons, Ltd.

KEYWORDS
wake model; eddy viscosity; wind turbine; wake predictions

Correspondence
Michael J. Werle, Ogin Inc., Waltham, Massachusetts 02453, USA.
E-mail: mjwerle@oginenergy.com
†Founder and Senior Technical Advisor

Received 12 March 2014; Revised 29 December 2014; Accepted 4 January 2015

NOMENCLATURE

a	non-dimensional flow field cross-sectional area
b	lateral scaling coefficient for eddy viscosity
c	cubic equation coefficient
C_P	turbine power performance coefficient
C_T	turbine total thrust coefficient
C_{TL}	local wake thrust/momentum deficit
C_t	rotor disc radial loading distribution
D	rotor diameter
h	turbine hub height
k_1, k_2	eddy viscosity empirical constants
P_T	total pressure
p	cubic equation coefficient
q	cubic equation coefficient
r	radial distance from the turbine centerline
R	non-dimensional radial distance measured in rotor radii, $R = 2r/D$
s	cubic equation coefficient
Ti	free-stream turbulence intensity in %
u	non-dimensional axial velocity
u_W	non-dimensional wake-averaged axial velocity

Copyright © 2015 John Wiley & Sons, Ltd.

V	axial velocity
x	axial distance downstream of turbine
X	non-dimensional axial distance downstream of turbine, $X = x/D$
Y	non-dimensional radial distance from the turbine centerline, $Y = r/D$
ν_T	non-dimensional eddy viscosity
ψ	non-dimensional stream function

Subscripts

CL	property evaluated on the centerline
E	property evaluated along the captured stream tube outer edge
min	minimum value
M	property evaluated in the mid-region of the rotor disc
O	property evaluated at the outlet plane of the near wake expansion region
r	property evaluated at the rotor
R	property evaluated in the root region of the rotor disc
T	property evaluated in the tip region of the rotor disc
w	property of the approaching wind speed
Outer	the outer edge of the wake mixing layer
Inner	the inner edge of the wake mixing layer
Upper	the region above the hub of the turbine
Lower	the region below the hub of the turbine

1. INTRODUCTION

As it is well documented, accurately predicting the productivity of wind farms is directly dependent on the ability to predict the wake of each wind turbine within that wind farm. As discussed by Barthelmie *et al.* [1,2], significant progress is being made in this regard, largely because of the recent emergence of high quality diagnostic-measured data and Computational Fluid Dynamic (CFD) calculations. However, there remains a need for a simple but reliable engineering model for accurately predicting the performance of a single turbine located in a sheared, turbulent, incoming wind velocity field.

Most engineering models in use today are based on, and/or are variants of, three models—the Jansen/Katic 'Top Hat' model [3,4], the Larsen asymptotic model [5,6] or the Ainslie eddy viscosity model.[7] Each of these contains empirical constants that have been tuned to certain cases and situations and, as such, inherently have limited ranges of applicability with significant uncertainty outside these ranges. Additionally, as they are currently formulated, they are unable to capture the influence of the rotor loading profile on the wake development. As noted by Barthelmie *et al.* [2] and Porte-Agel *et al.* [8], this seems to be critical to sufficiently representing the near wake (<2 rotor diameters downstream) and intermediate wake (2–4 rotor diameters downstream), which, in turn, sets the initial condition for the far wake (>4 diameters downstream). Larsen *et al.* [9] introduced a novel concept for addressing this shortfall within the context of the Ainslie eddy viscosity approach, but no validations of such appeared therein. Subsequent works, such as those by Madsen *et al.* [10], Keck *et al.* [11–13] and Larsen *et al.* [14], have focused on improvement, calibration and validation of this approach and various empirical modifications to the eddy viscosity model. Although their results have been encouraging, they have also added complexities and some accuracy uncertainties in predicting calculated and/or measured wake velocity profiles.

The goal of the current effort is to overcome some of the issues discussed earlier and provide an accurate, reliable, yet simple to apply, engineering model for a single turbine's wake. The approach used here builds from and enhances the modeling concepts of Larsen *et al.* [9] As such, it is another variant of the Ainslie eddy viscosity [7] approach. However, it pays special attention to four points:

1. first validating the key, but as yet unproven, assumption used in [9–14] that Froude's equation, linearly relating the wake and rotor plane velocities, applies for all radial points of the rotor disc with a non-constant but axisymmetric loading profile,
2. constructing a rational algebraic engineering model for representing a rotor's loading profile,
3. use of a simple viscous mixing model in the wake, and
4. incorporating a straightforward procedure for representing incoming wind shear influences.

As will be shown in the results below, the current model's predictions are directly applicable in both the intermediate and far wake regions.

Additionally, two figures of merit are employed herein to provide a consistent means of assessing the reliability of wake data and the flow mixing performance. The first, a wake momentum-flux or thrust parameter is used for quantitatively

assessing the accuracy, and thus utility of measured and/or computational wake data. It is known that this parameter must equal the turbine's total thrust coefficient at all downstream wake stations in the constant pressure mixing region. Failure to do so, as occurred in some cases analyzed herein, raises questions about the validity of the computational and/or experimental datasets.

The second figure of merit employed here is a rotor swept area wake-averaged velocity. As such, it represents the rotor's swept area-averaged velocity that dictates the performance of a downstream turbine. It is employed here as the primary quantitative measure for reliably assessing the wake's impact on a neighboring downstream turbine.

Through detailed comparisons with three independent state-of-the-art CFD solution datasets and a field measured dataset, the current model is shown to provide good engineering estimates for turbine rated power levels from 100 kW to 2.3 MW, wind speeds of 6 to 22 m s^{-1} and free-stream turbulence levels from 0% to 16%.

2. THE PARABOLIZED NAVIER–STOKES (PNS) THIN LAYER EQUATIONS AND THE EDDY VISCOSITY MODEL

Ainslie [7] and many others [15] have made direct use of the observed fact that aft of a turbine's near-wake region, wherein the pressure rises and the wake expands, the flow field enters a constant pressure region in which lateral diffusion and mixing dominate. Under these assumptions, the normally elliptic Navier–Stokes equations reduce to parabolic partial differential equations (i.e., the PNS equations) similar to the classic thin layer (TL) wake equations discussed by Schlichting [15] and Larsen *et al.* [5] and many others. The resulting equation set can be straightforwardly solved numerically once a means is established for setting the initial conditions and determining the analytical model for the turbulent mixing, usually modeled with an eddy viscosity approach. Numerous approaches have been employed for these; however, the current work follows that introduced by Larsen *et al.* [9]

The governing equations for the constant pressure region of the wake are given in terms of $X = x/D$ and $Y = r/D$ as follows:continuity

$$\frac{1}{Y}\frac{\partial}{\partial Y}(Yv) + \frac{\partial u}{\partial X} = 0, \tag{1}$$

axial momentum

$$u\frac{\partial u}{\partial X} + v\frac{\partial u}{\partial Y} = \left(\frac{v_T}{Y}\right)\frac{\partial}{\partial Y}\left(Y\frac{\partial u}{\partial Y}\right), \tag{2}$$

the eddy viscosity as

$$v_T = k_1 b(1 - u_{CL}) + k_2 T_i/100, \tag{3a}$$

where

$$b \equiv Y_{Outer} - Y_{Inner}. \tag{3b}$$

The shear layer thickness scaling coefficient, b of equations (3a) and (3b), varies at each axial location as the viscous shear layer spreads laterally. Likewise, the velocity deficit term, $1-u_{CL}$, in equation (3a), decreases axially once the shear layer spreads to the centerline. The constants k_1 and k_2 used by Larsen *et al.* [9] differed from those originally proposed by Ainslie [7] and were determined empirically from two separate numerical studies that provided $k_1 = 0.002$ and $k_2 = 0.001$. In [10–14], various 'filters' and adjustments were incorporated into the eddy viscosity model of equation (3a) in attempts to improve its wake related predictions of independent CFD and/or field-measured data. These adjustments have not been included in the current model as presented in the succeeding paragraphs, the implications of which are discussed later in Section 10.

For the current model, the shear layer thickness scaling, b of equation (3b), was taken as a constant over the length of the wake as follows:

$$b \equiv D_{OE}/2, \tag{4}$$

where D_{OE} is the diameter of the near wake outlet region (Figure 1). Additionally, the centerline velocity term, u_{CL} in equation (3a), was replaced with, u_{min}, the minimum velocity in the wake profile, to better scale the velocity differences promoting shear layer mixing. Finally, the empirical constants, k_1 and k_2 of equation (3a) were changed. It will be demonstrated in

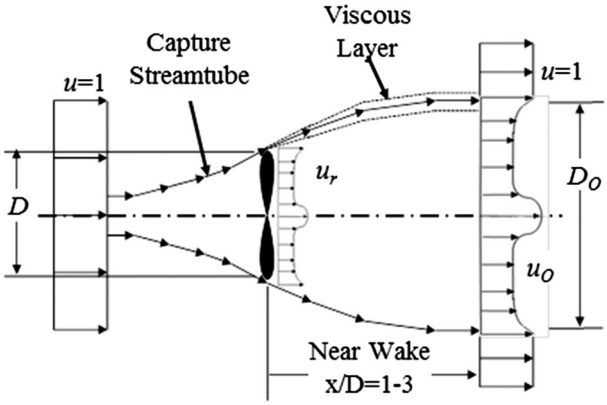

Figure 1. Near wake structure.

the following sections by setting $k_1 = 0.0005$ and $k_2 = 0.01$ in equation (3a), good comparison were obtained of the wake-averaged axial velocity downstream development for all of the 13 application cases considered herein.

Solution of equations (1)–(4) requires the input of initial u and v velocity profiles at some station x/D. Although numerous semi-empirical schemes have been employed by others with varying levels of success (for examples, see [7,16,17] and [18]), the current model employs a variant of that discussed by Larsen *et al.* [9] and [10–14] as provided in Sections 3 in the succeeding text.

3. VARIABLE LOAD ACTUATOR DISC MODEL

Larsen *et al.* [9] introduced the concept of employing a variable-load actuator-disc rotor model to initialize the PNS equations using the pressure expanded inviscid velocity profile one would expect at the downstream outlet end of the inviscid near wake as depicted in Figure 1. In [9], the rotor plane loading and related velocity profile, u_r, were first calculated from a Blade Element Momentum (BEM) model. This was then used in an analytical inviscid momentum balance model to determine the wake outlet velocity profile, u_O. This profile was then employed at $X = 0$ [9–14] as the initial condition for the PNS equation solutions in the constant pressure intermediate and far wake regions.

The Larsen *et al*. model [9] employed, as a key assumption (without proof), that Froude's equation,

$$u_r = \frac{1}{2}(1 + u_O), \tag{5}$$

applied along each streamtube of the near wake region. As this is, as yet, an unproven element of the analytical model, for completeness, a rigorous derivation of this generalized Froude equation is first provided here.

Applying the inviscid momentum and continuity equations in integral form from the constant pressure region upstream to the constant pressure region downstream of the rotor in Figure 1 allows one to relate the loading force on the rotor plane to the momentum flux at the downstream outlet plane through the following relation:

$$\int_0^1 C_t da_r = 2 \int_0^{a_{OE}} u_O \left(1 - u_O\right) da_O, \tag{6a}$$

where

$$a_r \equiv \frac{r_r^2}{(D/2)^2}, \tag{6b}$$

$$a_O \equiv \frac{r_O^2}{(D/2)^2}. \tag{6c}$$

Here, a_{OE} is the value of a_O at the outer edge of the capture streamtube and C_t is the non-dimensionalized local value of the disc total pressure loading, ΔP_T, which varies along the disc radius and is defined as follows:

$$C_t \equiv \frac{\Delta P_T}{\frac{1}{2}\rho V_w^2}. \tag{6d}$$

From Bernoulli's equation, it is known that along any streamline (or within any thin streamtube) in the inviscid near wake, the total pressure is a constant. With this, one can track any streamline through the rotor disc pressure drop to write from equation (6d) that

$$C_t = 1 - u_O^2, \tag{7a}$$

so that equation (6a) becomes

$$\int_0^1 \left(1 - u_O^2\right) da_r = 2 \int_0^{a_{OE}} u_O \left(1 - u_O\right) da_O. \tag{7b}$$

A stream function, ψ, is now introduced so that conservation of mass in a streamtube is maintained, allowing one to write that

$$d\psi = u_r da_r = u_O da_O. \tag{8}$$

With this, equation (7b) gives the following equation:

$$\int_0^{\psi_E} 2\frac{(1 - u_O)}{u_r}\left[u_r - \frac{1 + u_O}{2}\right] d\psi = 0, \tag{9}$$

which requires that along any streamline/streamtube, the integrand must be zero, i.e., Froude's equation (5) is thus proven applicable to each individual streamline/streamtube.

Combining equations (5) and (7) thus allows one to write that along the face of the rotor disc:

$$u_r = \frac{1}{2}\left[1 + \sqrt{1 - C_t}\right]. \tag{10}$$

The rotor and wake outlet velocity profiles can thus be determined for any loading profile, C_t, as discussed in the next section.

4. A SIMPLIFIED ROTOR LOADING MODEL

Larsen *et al.* [9], as well as.[10–14] used BEM calculations to determine the local rotor's loading profile, C_t, then equation (10) for u_r yielding a typical profile as depicted in Figure 1. Equation (6a) was thereafter solved iteratively to give the distribution of u_O at the outlet plane.

An alternate approach has been applied in the current model that allows one to bypass the BEM calculations and eliminate the iterative solution of equation (6a). To this end, it is first noted that horizontal axis wind turbine rotors are usually designed to carry a nearly constant loading over the majority of their core length (usually the Betz limit loading of $C_t = 8/9$) with a drop-off or deloading near the tip region and virtually zero loading in the root region. An idealized but simple-to-apply version of such a distribution is shown in Figure 2, where $R = 2r/D$ and in the root region where $R < R_R$,

$$C_t = 0, \tag{11a}$$

in the middle core region where $R_R < R < R_T$;

$$C_t = C_{tM} \tag{11b}$$

and in the tip region where $R_T < R < 1$; the loading is assumed to decay linearly with the flow area from its core value, C_{tM}, to zero at the tip, $R = 1$, as given by the following relation:

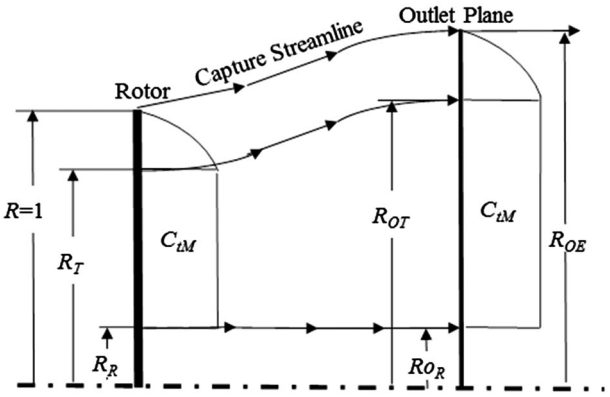

Figure 2. Idealized rotor's loading profile.

$$C_{\mathrm{t}} = C_{\mathrm{tM}} \frac{1 - R^2}{1 - R_{\mathrm{T}}^2}. \tag{11c}$$

The respective u_{r} distributions are then obtained directly from equation (10).

The velocity distribution at the outlet plane, u_{O}, can then be obtained by, first, using mass conservation between the two planes to write that

$$R_{\mathrm{OR}} = R_{\mathrm{R}}, \tag{12a}$$

and

$$R_{\mathrm{OT}} = \sqrt{R_{\mathrm{OR}}^2 + \frac{1}{2}\left[1 + \frac{1}{\sqrt{1 - C_{tM}}}\right]\left(R_{\mathrm{T}}^2 - R_{\mathrm{R}}^2\right)}, \tag{12}$$

With these, one can now write that in the lower region where $R < R_{\mathrm{OR}}$;

$$u_{\mathrm{O}} = 1, \tag{13a}$$

in the middle core region where $R_{\mathrm{OR}} < R < R_{\mathrm{OT}}$;

$$u_{\mathrm{O}} = \sqrt{1 - C_{tM}} \tag{13b}$$

and in the outer region where $R_{\mathrm{OT}} < R < R_{\mathrm{OE}}$, one can evaluate the integrals of equation (6a) to write that

$$u_{\mathrm{O}} = \sqrt{\left[4 - \left(1 + \sqrt{1 - C_{tM}}\right)^2\right] + 2C_{tM}\frac{R^2 - R_{\mathrm{OT}}^2}{1 - R_{\mathrm{T}}^2}}. \tag{13c}$$

Additionally, the rotor local C_{t} loading distributions of equations (11a)–(11c) lead to an expression for the total rotor trust coefficient, C_{T}, in terms of $a_{\mathrm{T}} = R_{\mathrm{T}}^2$ and $a_{\mathrm{R}} = R_{\mathrm{R}}^2$ as follows:

$$C_{\mathrm{T}} \equiv \int_0^1 C_t da_r = C_{\mathrm{tM}}\left[\frac{1}{2}(1 + a_{\mathrm{T}}) - a_{\mathrm{R}}\right] \tag{14a}$$

and the power coefficient as follows:

$$C_{\mathrm{P}} \equiv \int_0^1 C_t u_r da_{\mathrm{r}} = \frac{a_{\mathrm{T}} - a_{\mathrm{R}}}{2} C_{\mathrm{tM}}\left[1 + \sqrt{1 - C_{\mathrm{tM}}}\right] + \vartheta\left(1 - R_{\mathrm{T}}^2\right), \tag{14b}$$

where the last term of equation (14b) is a complex algebraic expression that is small for most rotors where R_{T} is near unity

and thus is ignored here. It is noted in passing that equations (14a) and (14b) revert to the classical one-dimensional actuator disc solution for $a_T = 1$ and $a_R = 0$. Additionally, it is recognized that for most modern turbines, the root region is small, such that $R_R < 0.2$ and $a_R < 0.04$.

Thus, with equations (10)–(13), it is seen that all the properties of the near wake depend principally on the mid-chord loading level, C_{tM}, and length of the tip deloading region, R_T. Through equations (14a) and (14b), the wake can also instead be characterized using the turbine's total thrust coefficients, C_T, and power performance coefficient, C_P. One immediate consequence of this is its implication that, because the near wake provides the initial conditions for the intermediate and far wake, one should expect to have to always employ at least two parameters to characterize the full wake.

5. INITIAL CONDITIONS AND THE PNS/TL CFD METHOD

A large number of solutions to date of the wake PNS/TL partial differential equations of Section 2 have initialized the computations at $X = x/D = 2$, where it is assumed the flow has reached a constant static pressure state. Many such methods use an empirically based Gaussian axial velocity profile of various forms.[7,17,18] However, as depicted in Figure 1, it is known that the near wake flow simultaneously experiences both inviscid expansion and viscous shear-layer mixing to establish the flow profile entering the constant pressure state, which may or may not start at $X = 2$. To represent this two-element, simultaneous process of expanding and mixing, the current model, like,[9–14] assumes instead, a two element/two-step tandem process. In the first step, the wake expands instantaneously to its outlet velocity profile of equations (13a)–(13c), which is imposed at $X = 0$ as shown in Figure 3. In the second step, this profile is then allowed to experience the viscous mixing throughout the near wake region.

For most turbines, it is unlikely that the rotor mid-chord loading level, C_{tM}, and/or deloading profile parameter, $a_T = R_T^2$, will be directly specified or easily determined. More likely, the system's power performance parameter, C_P, and turbine total thrust level, C_T, will be specified as in the numerous example cases presented in the following sections. For this reason, the current model first solves equations (14a) and (14b) for given values of C_P and C_T to determine the applicable values of C_{tM} and a_T, which are subsequently used in equations (12), (13a), (13b) and (13c) to establish the axial velocity profile at $X = 0$. For C_{tM}, equation (14a) gives the following:

$$C_{tM} = \frac{C_T}{\left[\frac{1}{2}(1 + a_T) - a_R\right]}. \tag{15a}$$

Inverting equation (14b) for a_T leads to the following cubic equation:

$$a_T^3 + pa_T^2 + qa_T + s = 0, \tag{15b}$$

where

$$p = \left[(1 - 2a_R)(3C_P/C_T - 4) + 2a_R + 2C_T^2/C_P\right]/[C_P/C_T - 2], \tag{15c}$$

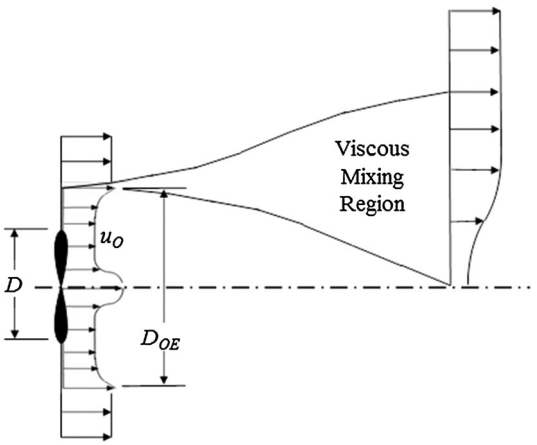

Figure 3. Initial conditions for current model.

$$q = \left[(1-2a_R)^2(3C_P/C_T - 2) + 4a_R(1-2a_R) - 4a_R C_T^2/C_P\right]/[C_P/C_T - 2] \tag{15d}$$

and

$$s = \left[(1-2a_R)^2((1-2a_R)C_P/C_T + 2a_R) + 2a_R^2 C_T^2/C_P\right]/[C_P/C_T - 2]. \tag{15e}$$

The well-known solution of equation (15b) is then given as follows:

$$a_T = \sqrt[3]{-\frac{c}{2} + \sqrt{\frac{c^2}{4} + \frac{d^3}{27}}} + \sqrt[3]{-\frac{c}{2} - \sqrt{\frac{c^2}{4} + \frac{d^3}{27}}} - p/3, \tag{15f}$$

where

$$d = \frac{1}{3}\left(3q - p^2\right) \tag{15g}$$

and

$$c = \frac{1}{27}\left(2p^3 - 9pq + 27s\right). \tag{15g}$$

For given values of C_P and C_T input to equations (15a)–(15g) and the resulting initial velocity profile, u_O, from equations (13a)–(13c), the PNS/TL equations (3a)–(6d) were solved numerically with boundary conditions at the centerline, $Y = R = 0$: $v = 0$

$$\frac{\partial u}{\partial Y} = \frac{\partial u}{\partial R} = 0, \tag{16a}$$

and at $Y = 10$:

$$u = 1. \tag{16b}$$

Appendix A provides details of the numerical scheme applied, including an estimate to the finite difference-generated error levels expected.

6. WAKE FLOW FIGURES OF MERIT

To date, nearly all wake flow studies have concentrated on providing the axial velocity profile across the full lateral wake region as it develops with distance aft of a turbine using either measured data, CFD-generated data or engineering models. Although these are informative and useful, they fail to provide a reliable yet simple and handy means of quantitatively assessing their accuracy and impact on a downstream turbine's performance. To address this shortfall, two easy to determine figures of merit will be employed in the example cases provided in the later sections.

For quantitatively assessing the accuracy and utility of wake measured and/or calculated data, a well-known wake related drag/thrust concept employed by Larsen,[7] Schlichting [11] and many others for modeling the constant pressure region of a wake, is invoked. To this end, it is first noted that an axial momentum and mass balance of the entire flow field from upstream of the turbine to any station in the downstream, constant pressure region, requires that the local value of the flow's momentum flux or thrust, C_{TL} as defined below, must be constant and equal to the turbine's total thrust, i.e.,

$$C_{TL} \equiv \int_0^\infty u(1-u)dR^2 = C_T. \tag{17}$$

It will be shown in the following applications that this is found to not always be the case for measured/calculated data and thus the validity of such datasets must therefore be judged accordingly.

For assessing the wake flow's impact on subsequent downstream turbines, use is made of the concept articulated by Barthelmie *et al.* [19] and employed in [10–14] that each turbine in an array performs according to its regular power and thrust curves evaluated at the 'local' wind speed seen just ahead of that turbine. For the current model, it is thus assumed that the meaningful performance figure of merit is the average velocity across the rotor's swept area because this is the portion of the wake that will deliver power to a downstream turbine. At each downstream station, this wake-averaged velocity over the turbine swept area is given by the following:

$$u_W \equiv \int_0^1 u dR^2 = 4\int_0^1 u dY^2. \tag{18}$$

The resulting axial distribution of u_W not only provides a simple quantitative measure of the wake mix-out rate, but it also provides an estimate of the effective wind velocity, and thus the C_T and C_P levels, a downstream turbine will deliver.

It is also noted here that Trolborg [20] proposed, as an alternate performance figure of merit, the use of the power integral across the wake swept area obtained by replacing u with u^3 in equation (18). In the current study, it was found that the value of u_W^3 from equation (18) provided virtually the same value as the power integral for all $X > 2$. Thus, one might equally employ either the definition of equation (18) or the cube root of the value proposed by Troldborg [20].

Note that use of u_W eliminates the confusion stemming from monitoring either the wake centerline velocity or the wake width as a primary figure of merit. In the rotor's root region, the rotor loading is nearly always near zero. Because of this, the centerline velocity in the near wake and intermediate wake region is always near unity—thus negating its usefulness for assessing the wake's mixing performance in the intermediate wake region as well as the early portion of the far wake region. Also, it is seen from equation (18) that only the core portion of the wake, i.e., where $R < 1$ as opposed to the full wake width, is of direct value and interest for assessing a downstream turbine's performance. Thus, the wake's total width is of secondary importance.

The following three sections apply the inputs of Sections 3–6 to wake predictions from the current model with comparisons to CFD calculations and field test data for a 100 kW, a 1 MW and a 2.3 MW turbine for a wide range of wind velocities and free-stream turbulence levels in the presence of incoming velocity profile shear.

7. WAKES FROM A 100 kW TURBINE

The CX-100 Sandia turbine has been extensively studied in performance and structural aspects [21,22] but not so for its wake. Duque [23] recently conducted an in-depth CFD study of CX-100 wakes, cosponsored by Ogin Energy and the US Department of Energy's Advanced Research Projects Agency-Energy (ARPA-E) Program,[24] using the AcuSolve code by AcuSim Inc. This code solves the unsteady Reynolds Averaged Navier Stokes (RANS) and Duque [23] showed excellent comparisons between his CFD calculations and field-measured performance data.[21,22] He employed two separate levels of rotor modeling, one using the exact blade geometry and the second using the load distributions from the first in an actuator line/disc model. The wake results [23] from the two rotor models were nearly indistinguishable; thus, only the latter were used here

The CFD wake results were presented [23] for wind speeds from 6 to 13.5 m s^{-1} at free-stream turbulence levels of 1% and 15%. The respective values of the turbine's power and thrust coefficients, C_P and C_T given in Table I, were then employed in equations (15a)–(15g) to calculate the comparable rotor loading values of C_{tM} and R_T, which were used in the current model. The results are shown in Figures (4)–(6) for an ambient turbulence level, $Ti = 1\%$.

Consideration will first be given to analyzing and qualifying the CFD results as these will provide a basis for assessing the current model predictions. Figure 4 shows the CFD-generated [23] velocity profiles at three representative axial stations

Table I. CX-100 parameters.

		Duque [23]		Equation (15)	
Ti	V_w (m s^{-1})	C_T	C_P	R_T	C_t
1%	6	0.700	0.439	0.890	0.818
	8	0.606	0.420	0.904	0.698
	10	0.524	0.379	0.899	0.606
	13.5	0.399	0.293	0.867	0.477
15%	6	0.699	0.439	0.890	0.817
	8	0.595	0.345	0.807	0.757
	10	0.506	0.316	0.809	0.643
	13.5	0.381	0.242	0.780	0.498

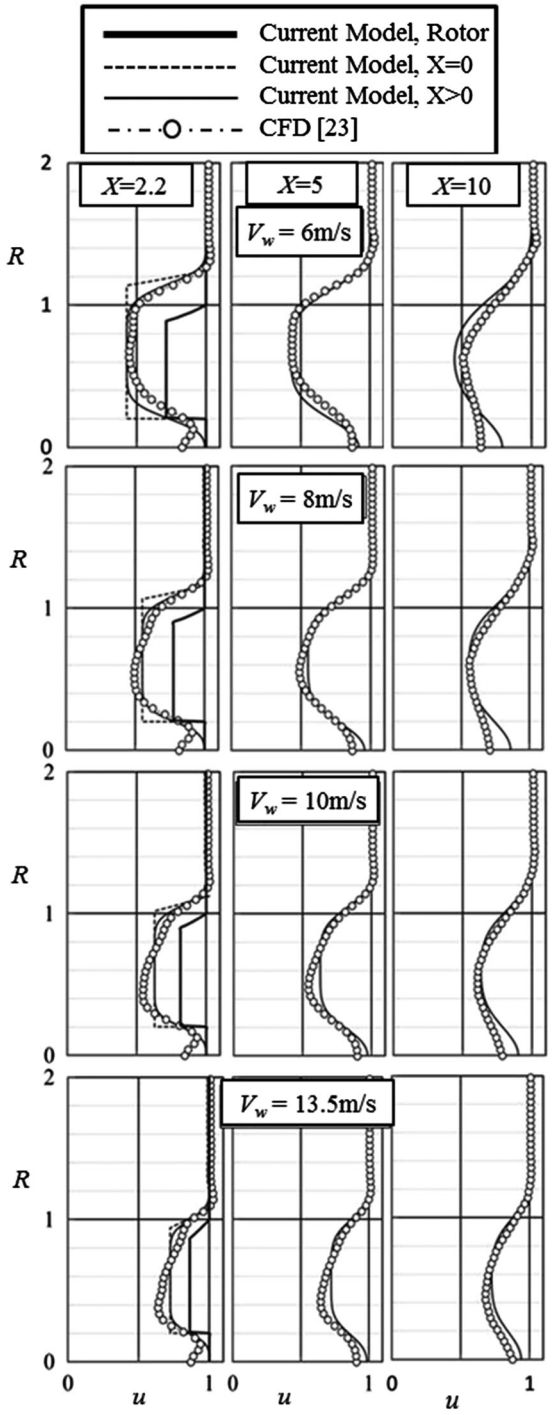

Figure 4. CX-100 wake profiles, $Ti = 1\%$.

and four wind speeds or loading conditions as listed in Table I. Velocity profiles were also provided [23] for $X < 2.2$ but none at the rotor plane, $X = 0$. Figures 5 and 6 provide the accompanying wake and performance figures of merit, C_{TL} and u_W, for five representative wake locations. Note is made of three aspects of the velocity profiles:

1. The CFD loading profiles, as reflected by those shown at $X = 2.2$, show the general attributes of the current model—low loading in the root and tip regions with relatively uniform loading otherwise.

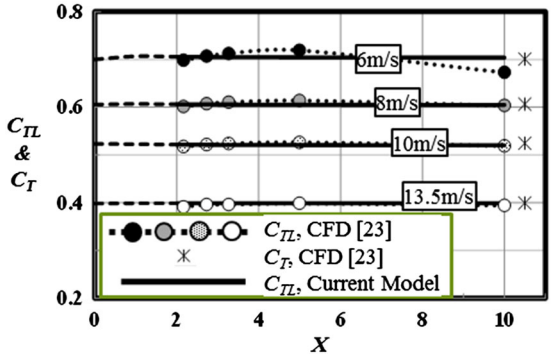

Figure 5. CX-100 wake thrust, $Ti = 1\%$.

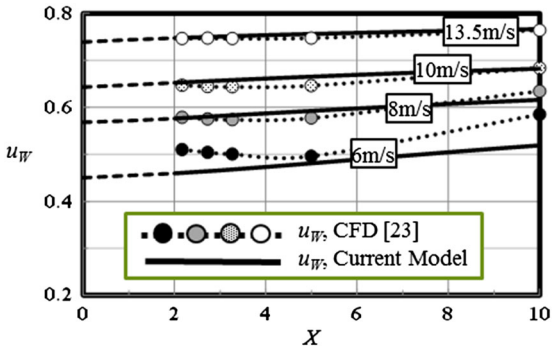

Figure 6. CX-100 wake-averaged velocity, $Ti = 1\%$.

2. They all show centerline velocity values significantly higher than the core values, even at $X = 10$, apparently because of the low level turbulent mixing, i.e., $Ti = 1\%$.
3. They all show a significantly thick outer edge sheared mixing layer that does not reach to the centerline—thus, none of the profiles seems to ever reach the classical Gaussian asymptotic velocity profile or far wake region.

The CFD-generated velocity profiles [23] were used in equation (17) to determine the axial variation of the wake figure of merit, C_{TL}, as shown in Figure 5. Also shown to the right side of the graph are the accompanying CFD-generated values of C_T given in Table I. It is reasonable to expect that the values of C_{TL} would monotonically approach the C_T values from below as the wake enters its constant pressure mixing region. Although this seems to be the case for the high-wind speed/low-loading case, small anomalies begin to appear as the wind velocity decreases and the loading increases. Values of C_{TL} greater than C_T indicate an improper inflow of momentum into the wake, apparently because of numerical errors in the CFD methodology. All cases are seen to ultimately come close but be slightly less than their respective C_T values except the $6\,\mathrm{m\,s^{-1}}$ case, which shows a significant drop in value at $X = 10$—indicating a significant numerical leakage of momentum from the wake. These observed behaviors indicate that the CFD results likely provide quantitative benchmark values for the low and intermediate loading cases but must be considered of only qualitative value for the highest load case.

The accompanying distributions of the performance figure of merit, u_W, from equation (18) are shown in Figure 6, where one first notes their very slow growth/recovery rate toward unity, again apparently because of the low level of turbulent mixing. Base on the Figure 5 results and discussion earlier, it is believed that these do provide reasonably accurate quantitative benchmark values for all but the $6\,\mathrm{m\,s^{-1}}$ case that is more of qualitative value.

The results from the current model are also shown in Figures 4–6. In Figure 4, it is seen that for each wind speed, the first panel ($X = 2.2$) also provides the current model's rotor profile, u_r, and the initial profile, u_O, that was applied at $X = 0$. The observed significant change from the u_r profile to the u_O profiles for all four cases indicates the level of changes one should expect in the near wake region. In all cases, the current model profiles reasonably well match the CFD profiles for from $X = 2.2$ to 10, especially in the important core and outer reaches of the wake. The centerline values do not match the CFD results as well, but, while esthetically less pleasing, this is of little quantitative consequence because so little power is contained in the root area of the turbine.

The current model's local thrust, C_{TL}, results are seen in Figure 5 to be essentially constant from $X = 0$ to 10 and very near the input C_T values, as they should be. They generally vary by less than 1% with slightly higher deviations near $X = 0$ apparently because the numerical errors generated resolving discontinuities in the u_O profile gradiants. As indicated

in the Appendix, a finite difference truncation error analysis conducted at $X = 5$ indicates the results are likely within 1% of the exact solutions and thus provide a good engineering estimate. Note also that the current results are shown as dashed lines for $X < 2$ to indicate they are not applicable in this region. They provide valid solutions to the current model's governing equations, which themselves are not valid in this region. Otherwise, the results compare qualitatively and quantitatively very well with the CFD results with the exceptions noted earlier for the 6 m s^{-1} case. It should be kept in mind that the values used here for the current eddy viscosity model constants, k_1 and k_2 of equation (3a) have been set based on collectively achieving good comparisons with the CFD-generated results of this case and the nine others cases presented in the succeeding paragraphs.

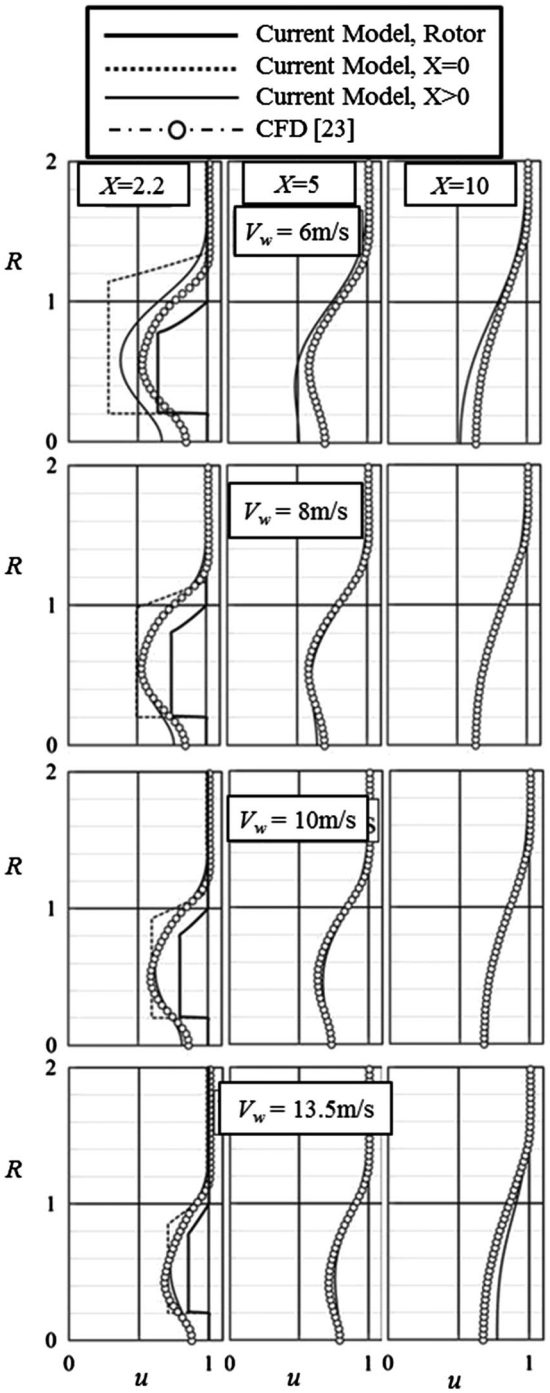

Figure 7. CX-100 wake profiles, $Ti = 15\%$.

Figure 6 shows the comparison of the related wake-averaged velocities, u_W, from the current model calculations. Similar to the CFD results, they display a strong variation of u_W with wind speed (or turbine thrust coefficient, C_T) but a slow growth with wake distance, X, for all but the already noted anomalous case of 6 m s^{-1} at $X = 10$. It is seen that overall behavior pattern and quantitative levels of the CFD results are seen to be reproduced reasonably well by the current model for nearly all cases.

Results for a free-stream turbulence level of 15% are shown in Figures 7–9. Again, first giving consideration to qualifying the CFD results, comparison of Figures 4 and 7 for respective turbulence levels of 1% and 15% show, as expected, dramatic changes in the profile shapes and mix out rates at similar values of wind speed, V_w. Here, the root and tip region shear layers are thicker and more or less merge aft of $X = 2.2$. At $X = 10$, the profiles are all very similar and of the asymptotic Gaussian shape.

The accompanying values of C_{TL} and C_T are shown in Figure 8. All show an orderly axial variation and growth toward their final values as they should, thereby implying a high degree of reliability for this dataset. Because of the higher turbulence level, the resulting u_W variations given in Figure 9 display faster growth and higher values than their counterparts in Figure 6.

Turning attention now to the current model's velocity profile predictions in Figure 7, note is first made that the initial u_O profiles differ from those of Figure 4 at the same values of wind speed. This is because of the different values of C_P for $Ti = 1\%$ and 15% provided in [23] and shown in Table I for nearly the same values of turbine total thrust, C_T. Through the determination of the tip deloading area, a_T, and the core disc loading level, C_{tM}, from equations (15a)–(15g), this significantly changes the rotor's loading profile, thus the u_O profile and thereafter the wake profile.

In Figure 7, it is seen that for $Ti = 15\%$ the current model virtually reproduces the CFD velocity profiles at all stations for V_w from 8 to 13.5 m s^{-1} (C_T from 0.4 to 0.6 in Table I). For $V_w = 6$ m s^{-1} ($C_T = 0.7$), the current method's velocity profile mix-out rate lags that of the RANS CFD but is seen to be catching up to it aft of $X = 5$. This is reinforced in Figure 8, which shows that for $V_w = 6$ m s^{-1}, the CFD wake only enters the constant pressure, constant local thrust state aft of $X = 5$. All the other cases do so near $X = 2.5$.

For $Ti = 15\%$, the current model's predicted local thrust levels, C_{TL}, are seen in Figure 8 to be near constant for all, but the low velocity, high total thrust case for $X < 2$, again, apparently because of numerical errors produced resolving the

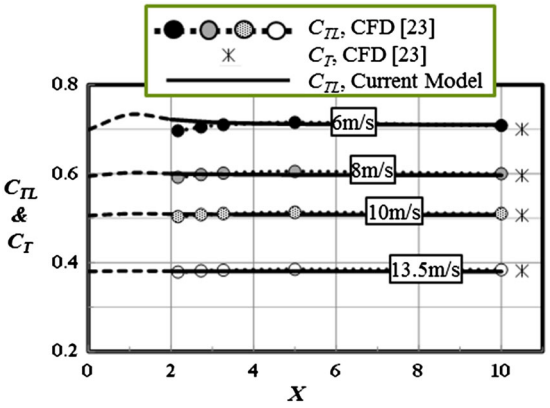

Figure 8. CX-100 wake thrust, $Ti = 15\%$.

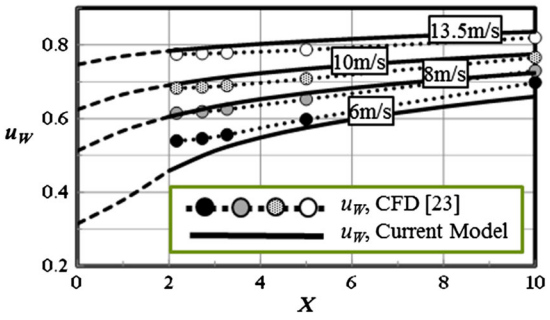

Figure 9. CX-100 wake-averaged velocity, $Ti = 15\%$.

rather severe discontinuities in the u_O profile gradients shown in the top panel of Figure 7. As indicated in Figure 8, this case recovers to the correct value for $X > 4$.

Figure 9, shows that the current model predictions of the wake-averaged velocity axial evolution for $Ti = 15\%$ reasonably match the CFD results qualitatively and quantitatively for all cases without the use of any of the eddy viscosity model filters and adjustments proposed in.[10–14] They slightly under predict u_W for $V_w = 6\,m\,s^{-1}$ and slightly over predict it for all the other values of V_w.

8. WAKES FROM A 1 MW TURBINE

Troldborg's dissertation [20] has provided a very detailed and thorough LES CFD study for the 1-MW Tjaereborg turbine using an Actuator Line BEM method to represent the rotor aerodynamics. He conducted a systematic study of a wide range of factors influencing the turbine's wakes, including those due to varying wind velocity, the free-stream turbulence level and incoming velocity shear level for single and multiple turbine configurations.

For the single turbine configuration considered here, Troldborg provided CFD-generated wake axial velocity profiles for wind speeds, $V_w = 10$, 14 and $22\,m\,s^{-1}$ with $Ti = 0\%$ and for $10\,m\,s^{-1}$ at $Ti = 9\%$. The associated CFD-generated C_P values, reproduced here in Table II, were shown to compare very well with field measurement data. Troldborg also provided CFD results for $V_w = 6\,m\,s^{-1}$, which were found here to have a wake data figure of merit, C_{TL}, greater than one. This would indicate the turbine had extracted more than the incoming total pressure from each streamline, which is not possible. Thus, this case has been excluded from the current analysis.

Figure 10 shows the wind speed (or loading) impacts on the variations in the $Ti = 0\%$ CFD wake velocity profiles for $X = 0$, 3, 5 and 7. The accompanying CFD-generated C_{TL} and C_T values are shown in Figure 11(a). It is seen that Troldborg's CFD results indicate a small momentum influx into the wake for $X > 2$ for $V_w = 14\,m\,s^{-1}$ and a more significant one for $V_w = 10\,m\,s^{-1}$. The resulting wake performance figures of merit, u_W, are shown in Figure 11(b). All the results, except those for $10\,m\,s^{-1}$, indicate a high level of consistency and thus provide valid benchmarking data. The $10\,m\,s^{-1}$ case can only be considered of qualitative utility.

The current predictions provided in Figure 10 were generated using Troldborg's [20] power performance coefficients, C_P, and total turbine thrust, C_T, values (Table II) along with an assumed value of the rotor's root radius, $R_R = 0.2$, in equation (15) to set the initial, u_O, profiles. Note that the current models simplistic rotor's loading profile, u_r, is also shown to compare well with the BEM-based [20] rotor velocity profiles. Additionally, the current models wake profiles are seen to essentially reproduce the CFD results for all but $V_w = 10\,m\,s^{-1}$ at $X = 7$, which likely is related to the erroneous momentum influx discussed earlier for this case.

As shown in Figure 11, the current model's C_{TL} and u_W predictions are seen to match very well with the CFD results for $X > 2$, except for the CFD-calculated anomalies noted earlier for $10\,m\,s^{-1}$.

Troldborg [20] also provided one CFD case for a free-stream turbulence level of $Ti = 9\%$ at $V_w = 10\,m\,s^{-1}$. However, as shown in Figure 12, the current analysis of his CFD velocity profiles showed a large erratic variation of the data figure of merit, C_{TL}, along the wake development path, thereby severely compromising the quantitative value of the results. The current model's predictions are seen to experience an increase in C_{TL} for $X < 2$ again, apparently, because of difficulty in numerically resolving the gradiant discontinuities in the velocity profiles at the initial station.

Finally, Troldborg [20] also provided CFD solutions for cases with significant shear across the incoming wind velocity profile for $Ti = 0\%$ and 9% as shown in Figure 13. These are of interest to this study because they raise the question of how to relate the current axisymmetric model to this more typical situation where the presence of a ground plane and velocity shear introduce three dimensional effects.

The left side panel of Figure 13 shows Troldborg's [20] imposed wind velocity profile, V_w, as well as his calculated rotor plane velocity profiles, which were the same for $Ti = 0\%$ and 9%. The right hand panel shows examples of the resulting CFD wake profiles at $X = 5$ for the two turbulence levels. Wake profiles were also provided at $X = 3$ and 7 with similar results.

Table II. Tjaereborg 1 MW parameters.

		Troldborg [20]		Equation (15)	
Ti	V_w ($m\,s^{-1}$)	C_T	C_P	R_T	C_t
0%	10	0.800	0.510	0.949	0.879
	14	0.560	0.400	0.904	0.645
	22	0.140	0.119	0.898	0.162
9%	10	0.800	0.510	0.949	0.879

DOI: 10.1002/we

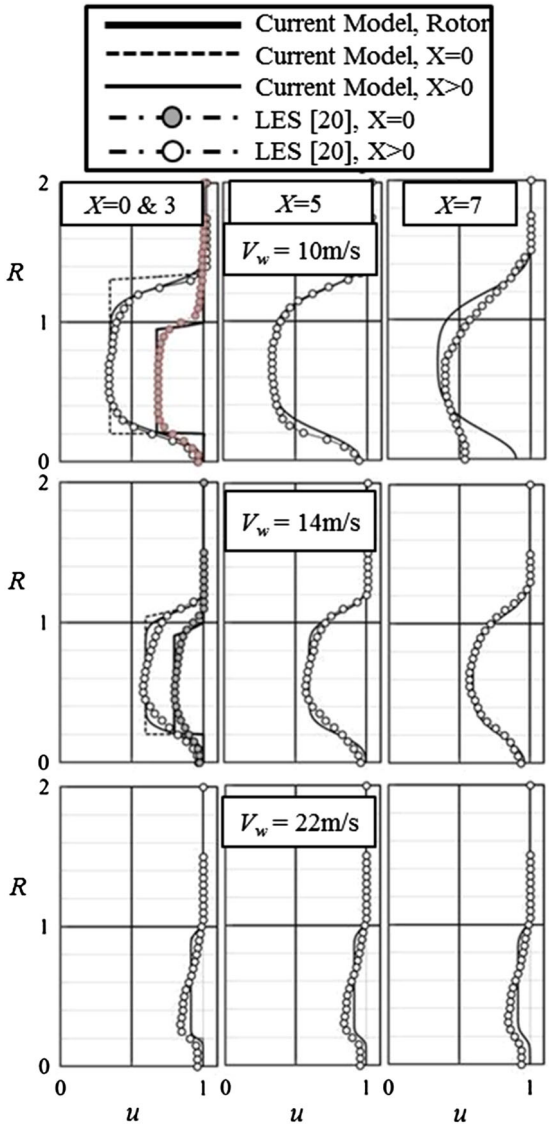

Figure 10. Tjaereborg 1 MW wake profiles, $Ti = 0\%$.

The influence of the ambient turbulence on the wake profiles is seen to be quite large as the deficit drops by nearly 50% for *Ti* increasing from 0% to 9%. Also, as Troldborg noted, a speedup of the wake velocity higher than that of the local wind velocity occurs at $X = 5$ near the surface (i.e., $R = 2h/D < 0.9$ in Figure 13) because of the vertical expansion of the wake's core flow area.

To relate these results to the current model, an observation made by Chamorro *et al.* [25] is first invoked. In a very detailed and refined set of wind tunnel experiments focused on wind turbine wakes, they provided convincing evidence that wakes in the presence of a sheared flow profile over a ground plane can be viewed as an axisymmetric wake superimposed on a two dimensional sheared flow. Applying that concept allows one to write that

$$u = \frac{V_{\mathrm{w}} - V}{V_{\mathrm{wHub}}} + 1. \tag{19}$$

Figure 14 shows the results from application of equation (19) to the CFD data of Figure 13 for the upper portions of the profiles where $R = 2h/D > 2$ and the lower portions where $R = 2h/D < 2$. It is seen that at $X = 0$, the rotor upper and lower profile portions are virtually identical, thus validating the superposition hypothesis of Chamorro *et al.* At $X = 5$, the upper

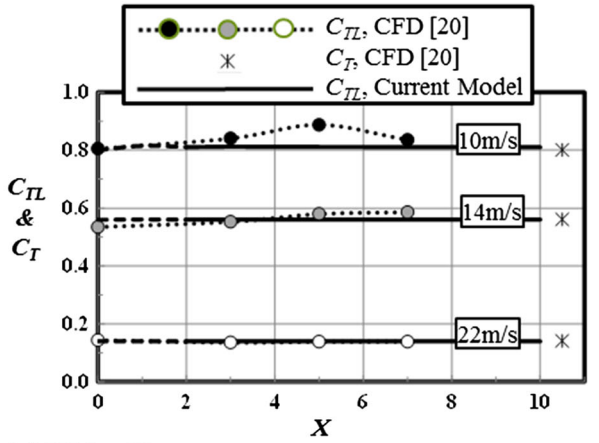

(a) Wake Thrust

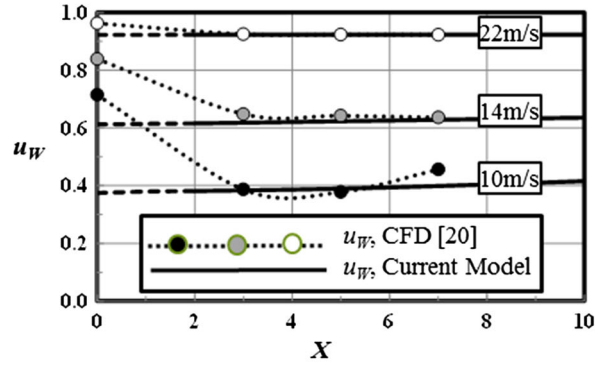

(b)Wake Averaged Velocity

Figure 11. Tjaereborg 1 MW turbine, $Ti = 0\%$.

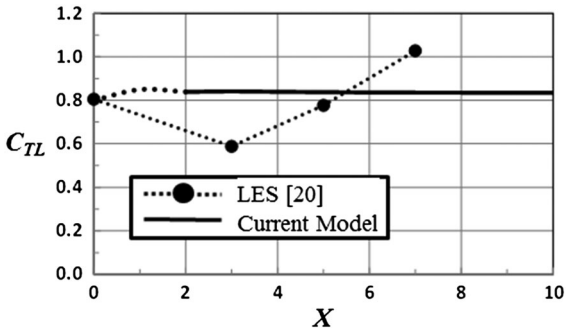

Figure 12. Tjaereborg 1 MW turbine, $Ti = 9\%$.

and lower profiles for $Ti = 9\%$ are nearly identical while those for $Ti = 0\%$ differ, apparently, because of the larger wake expansion-induced speed up effect noted in Figure 13. For comparison, the axisymmetric profiles for the No Shear cases from Figure 10 are also shown at $X = 5$, indicating good qualitative and quantitative comparisons. The real test of this concept, however, are the values of u_W it delivers. For current purposes, it is assumed that the wake velocity speedup only occurs in the lower quadrant of the wake and that the upper profile applies in the remaining three quadrants. This leads to a weighted-average value equal to 25% of u_{WLower} plus 75% of u_{WUpper}. Figure 15 compares the resulting values with their axisymmetric counterparts for $Ti = 0\%$ and 9%. The excellent agreements shown for the cases with shear and without shear are a strong confirmation of Chamorro *et al.* [25] premise and thus is taken as confirmation of the applicability of the current method for modeling wind turbines in sheared wind streams.

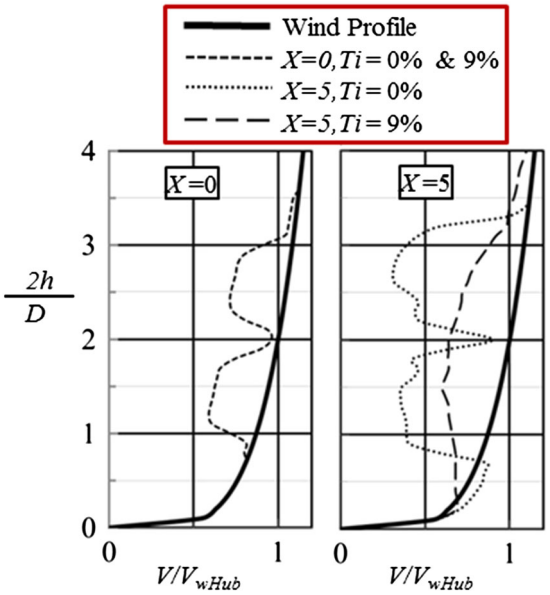

Figure 13. Tjaereborg 1 MW sheared wake profiles.

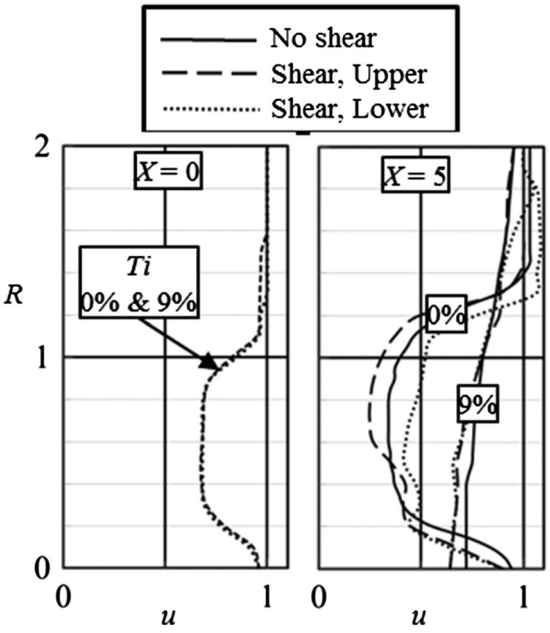

Figure 14. Tjaereborg 1 MW wake profiles.

9. THE WAKE OF A 2.3 MW TURBINE

Porte-Agel *et al.* [8] conducted LES (Large Eddy Simulation) CFD studies of an array of small wind turbines placed in wind tunnels and of a 2.3 MW Siemens turbine located in Mower County Minnesota, USA. For the 2.3 MW turbine case, Sodar data was taken [26] ahead of and 4.25 diameters downstream of the turbine as shown in Figure 16. Three actuator disc models were used with a BEM methodology to determine the flow conditions at the rotor plane; a nonrotating, evenly loaded actuator disc, a rotating, distributed load rotating actuator disc and a distributed load actuator line. It was found that the latter two provided very similar and the best comparisons with measured data; thus, it is the result shown in Figure 16.

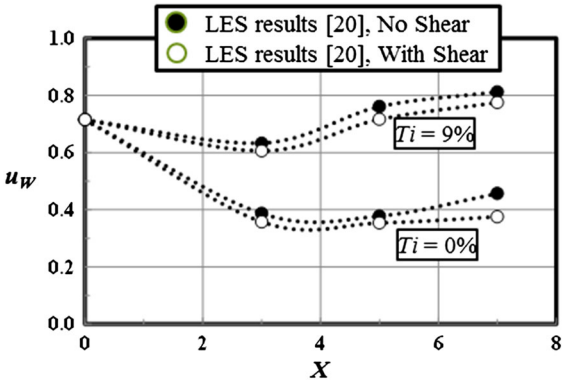

Figure 15. Tjaereborg 1 MW turbine with velocity shear.

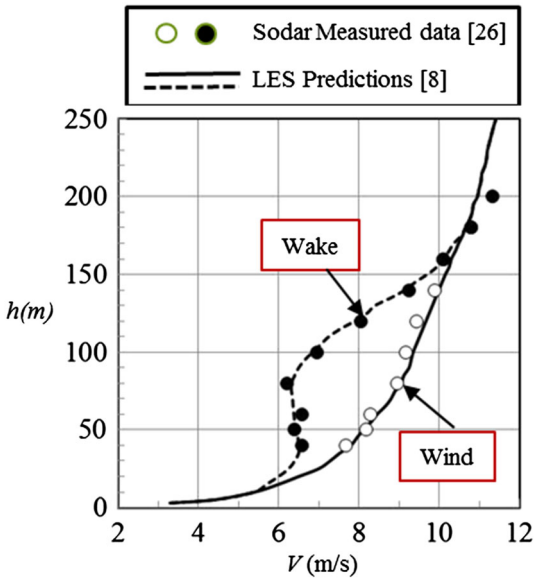

Figure 16. Siemens 2.3 MW turbine performance.

Using the superposition approach discussed in Section 8 earlier, the measured upper and lower axial velocity profiles, u, were determined from the data of Figure 16 using equation (19). As seen in the top panel of Figure 17, indicated by the open and filled circles at $X = 4.25$, the two profiles were very similar with a slight amount of speedup evident in the lower profile. The CFD calculation results are also shown as the open and filled squares in the upper panel of Figure 17, showing slightly lower velocity deficits than the data. However, for these calculations, while the power performance coefficient value of $C_P = 0.461$ was provided by the Scada system,[8] the turbine total thrust value, C_T, was not available. Porte-Agel *et al.* [8] therefore used the calculated average rotor speed and a uniformly loaded actuator disc model with zero deloading in the tip or root regions, i.e., $R_T = 1$ and $R_R = 0$, to calculate a $C_T = 0.552$. When these values of C_P and C_T were used with the current method, they produced the slightly larger velocity deficits shown in the upper panel of Figure 17. Upon interrogating these results further, it was found that the Sodar-measured wake data shown in Figure 17 indicated a $C_T = C_{TL} = 0.504$, 10% less than that employed by Porte-Agel *et al.* Current solution results generated employing this lower C_T value are shown in the bottom panel of Figure 17 to better represent the measured data. The wake-averaged velocity values for this latter case were $u_W = 0.77$, while the measured data gave $u_W = 0.79$.

10. CONCLUDING REMARKS

The current variant of the Ainslie eddy viscosity wake model has been shown to be applicable over a wide range of turbine ratings (100 kW–2.3 MWs), wind velocities (6–22 m s^{-1}) or thrust levels ($C_T = 0.14$–0.8), and turbulence levels (0–16%). It

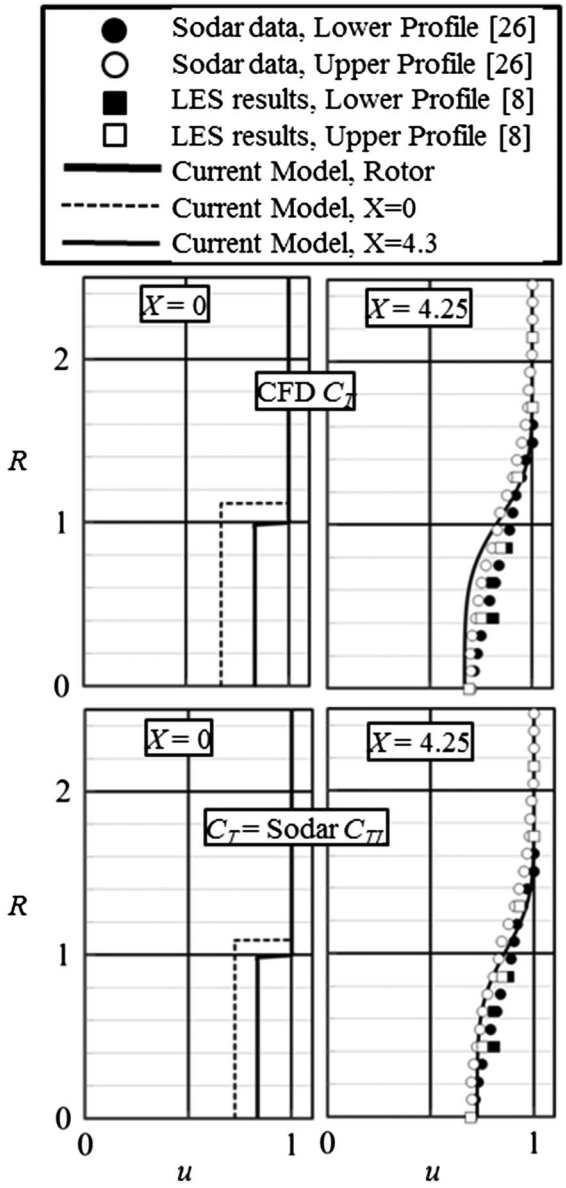

Figure 17. Siemans 2.3 MW turbine wake profiles, $Ti = 16\%$.

provides solutions comparable with those provided by both state-of-the-art RANS and LES CFD solutions as well as Sodar measured field data. Its two-parameter representation, using the turbines power performance coefficient, C_P, and its total thrust coefficient, C_T, was found to sufficiently represent the rotor's loading profile and subsequently capture the wake development up to 10 diameters downstream. Going forward, it is therefore recommended that both C_T and C_P be directly recorded in all wake-related measurement or computational campaigns.

Evidence was also provided here that the velocity profile superposition hypothesis of Chamorro *et al.* was verified for typical sheared free-stream flows—i.e., that the wake of a single turbine up to 10 diameters downstream generally develops as an axisymmetric process superimposed on an otherwise two-dimensional sheared velocity field. As shown herein, a slight accommodation for the ground plane-induced velocity speedup in the wakes' lower quadrant is warranted.

The two quantitative figures of merit adopted herein, the wake momentum flux/thrust data parameter, C_{TL}, and the swept area wake-averaged velocity performance parameter, u_W, were shown to provide important information for assessing the reliability of datasets and wake impacts. First, it is critical that the locally determined values of C_{TL} (either measured or calculated) attain the measured rotor C_T value within a few diameters downstream of the turbine. It must hold that value throughout the wake. If this is found to not be the case, the quantitative value of the data must be questioned. For both measured and calculated wakes, the important measure of the wake flow's impact on a downstream turbine's performance is

contained in the u_W value just ahead of that turbine, and the integrity of that value depends directly on the degree to which $C_{TL} = C_T$ along the length of the wake.

There remains an open question concerning the eddy viscosity model used herein as compared with those adjusted models put forth by Larsen, Madsen and Keck *et al.* [10–14], i.e., which, if any, is best for obtaining reasonably accurate engineering estimates of wake influences and impacts? At this point, there seems to be two important points to keep in mind: (i) any of the adjusted models can be easily inserted in the current methodology and (ii) there is yet too little qualified field data to make such a final determination.

APPENDIX A

CFD Method

In the current study, the governing equations given by equations (1)–(3b), were solved using a standard first order accurate implicit finite difference scheme from the rotor plane, $X = 0$–10 with a lateral domain width also from $Y = 0$–10. The lateral step size used was $\Delta Y = 0.001$, and the axial step size used was $\Delta X = 0.1$. This latter value was established based on results of a step-size error analysis. As shown in Figure A1, the value of u_W at $X = 5$ calculated with the current method for the 100 kW CX-100 turbine studied by Duque [18] is seen to approach a linear dependence for $\Delta X < 0.15$ as it must to be truly first order accurate. As shown in Figure A1, the resulting linear extrapolation then implies an error of less than 1% at $\Delta X = 0.1$.

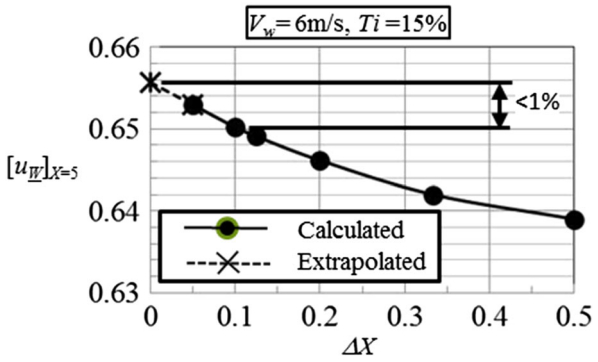

Figure A1. CX-100 turbine, current model step size study.

REFERENCES

1. Barthelmie R, Fokerts G, Larsen GC, Rados K, Pryor S, Frandsen S, Lange B, Shepers JG. Comparison of wake model simulations with offshore wind turbine wake profiles measured by sodar. *Journal of Atmospheric and Oceanic Technology* 2006; **23**: 888–901.
2. Barthelmie R, Larsen GC, Pryor S, Jorgensen H, Bergstrom H, Maggnusson M, Schlez W, Rados K, Lange B, Volund P, Neckelman S, Morgensen S, Shepers JG, Hegberg T, Fokerts G. Efficient Development of Offshore Wind Farms (ENDOW), Riso National Laboratory Report R-1407(EN), April 2003.
3. Jensen NO. A Note on Wind Generator Interaction", Risø National Laboratory Report-M-2411, 1984.
4. Katic I, Højstrup KJ, Jensen NO. A simple model for cluster efficiency, *European Wind Energy Association Conference and Exhibition*, Rome, Italy, 7–9 October 1986.
5. Larsen GC. A simple wake calculation procedure, Riso National Laboratory Report RISO-M-2760, 1988.
6. Larsen, G.C., Madsen, H.A., and Sorensen, N.N., Mean Wake Deficit in the Near Field, European Wind Energy Conference, 2003.
7. Ainslie JF. Calculating the flowfield in the wake of wind turbines. *Journal of Wind Engineering and Industrial Aerodynamics* 1988; **27**: 213–224.
8. Porte-Agel F, Wu Y, Lu H, Conzemiou RJ. Large-eddy simulation of atmospheric boundary layer flow through wind turbines and wind farms. *Journal of Wind Engineering and Industrial Aerodynamics* 2011; **99**: 154–168.
9. Larsen GC, Madsen HA, Larsen TJ Troldborg N. Wake modeling and simulation, RiSO National Laboratory Report RISO-R-1653(EN), July 2008.

10. Madsen HAa, Larsen GC, Larsen TJ, Troldborg N. Calibration and validation of the dynamic wake meandering model implemented in the aeroelastic code HAWC2. *Journal of Solar Energy Engineering* 2010; **132**: 041014-1—041014-14. DOI: 10.1115/1.4002555.
11. Keck RE, Veldkamp D, Madsen HAa, Larsen GC. Implementation of a mixing length turbulence formulation into the dynamic wake meandering model. *Journal of Solar Energy Engineering* 2011; **134**: 021012-1—021012-13.
12. Keck RE, de Maré M, Churchfield MJ, Lee S, Larsen G, Madsen HAa. On atmospheric stability in the dynamic wake meandering model. *Wind Energy* 2013, DOI: 10.1002/we.1662.
13. Keck RE, de Maré M, Churchfield MJ, Lee S, Larsen G, Madsen HAa. Two improvements to the dynamic wake meandering model: including the effects of atmospheric shear on wake turbulence and incorporating turbulence build up in a row of wind turbines. *Wind Energy* 2013, DOI: 10.1002/we.1686.
14. Larsen TJ, Madsen HAa, Larsen GC, Hansen KS. Validation of the dynamic wake meander model for loads and power production in the Egmond aan Zee wind farm. *Wind Energy* 2012; **16**: 605–624 DOI: 10.1002/we.1563
15. Schlichting H, Boundary Layer Theory, Fourth Edition. McGraw Hill Inc: New York, 1960, p 604.
16. Sanderse B, van der Pijk SP, Koren B. Review of Computational fluid dynamics for wind turbine wake aerodynamics. *Wind Energy* 2011; **14**: 799–819.
17. Renkema D. Validation of wind turbine wake models using wind farm data and wind tunnel measurements, Thesis, Delft Technical University, 2007.
18. Anderson M. Simplified solution to the eddy-viscosity wake model, renewable energy systems tech. Report #01327-000202. 2nd ed., 2009
19. Barthelmie R, Jansen LE. Evaluation of wind farm efficiency and wind turbine wakes at the Nysted offshore wind farm. *Wind Energy* 2010; **13**: 573–586, DOI: 10.1002/we.408.
20. Troldborg N. Actuator line modeling of wind turbine wakes, PhD Thesis, Technical University of Denmark, June 2008.
21. Berry DS. Blade system design studies phase II, final project report, SANDIA REPORT SAND2008-4648, July 2008.
22. Zayas JR, Johnson WD. 3X-100 blade field test, SANDIA REPORT SAND2007-5138, March 2008, also By personnel communication between Earl Duque and Jonathan C. Berg, Sandia National Laboratory-Albuquerque, NM, USA
23. Duque EPN. Wind tunnel wake study, task 2-final report, intelligent light corporation applied research group, Doc. No. IL-ARG-FloDesign-Final Report 100203, Feb 2011.
24. Werle MJ. Wind turbine wake model assessments, FloDesign Wind Turbine Corp. Report FDWT-0055, Nov. 2011.
25. Chamorro LP, Porte-Agel F. A wind tunnel investigation of wind turbine wakes: boundary-layer turbulence effects. *Boundary Layer Meteorology* 2009; **132**: 129–149.
26. Conzemius B, Lu H, Chamorro L, Wu Y, Porte-Agel F. Development and testing of a wind farm simulator at an operating farm, WindLogics/Univ of Minn presentation in 2010 downloaded, Sept 20 2013.